Journal of Non-Crystalline Solids 554 (2021) 120614

Contents lists available at ScienceDirect

Journal of Non-Crystalline Solids

journal homepage: www.elsevier.com/locate/jnoncrysol

Rigidity theory of glass: Determining the onset temperature of topological constraints by molecular dynamics

Yushu Hu [a], Zegao Liu [a], Kai Yang [a], N M Anoop Krishnan [b,c], Morten M. Smedskjaer [d], Gaurav Sant [e,f,g], Mathieu Bauchy [a,g,*]

[a] Physics of AmoRphous and Inorganic Solids Laboratory (PARISlab), University of California, Los Angeles, California, 90095, USA
[b] Department of Civil Engineering, Indian Institute of Technology Delhi, Hauz Khas, New Delhi 110016, India
[c] Department of Material Science and Engineering, Indian Institute of Technology Delhi, Hauz Khas, New Delhi 110016, India
[d] Department of Chemistry and Bioscience, Aalborg University, 9220 Aalborg, Denmark
[e] Laboratory for the Chemistry of Construction Materials (LC2), Department of Civil and Environmental Engineering, University of California, Los Angeles, California, 90095, USA
[f] Department of Materials Science and Engineering, University of California, Los Angeles, California, 90095, USA
[g] Institute for Carbon Management, University of California, Los Angeles, California, 90095, USA

ARTICLE INFO

Keywords:
Topological constraint theory
Glass transition temperature
Molecular dynamics

ABSTRACT

Topological constraint theory has been extensively used to describe how the composition and structure of glasses and glass-forming melts control their properties. This approach relies on an accurate enumeration of the topological constraints acting in the atomic network. Such direct enumeration is challenging since constraints can be active or thermally-broken depending on temperature. Here, based on molecular dynamics simulations, we present a generic method aiming to predict the onset temperature below which constraints become active. We illustrate this method by considering the example of a series of binary calcium silicate glasses. We find that inter-polytope angular bond-bending constraints are associated with a lower onset temperature than intra-polytope angular constraints. Based on this, we show that the differing values of these two onset temperatures largely govern the glasses' fictive temperature.

1. Introduction

Topological constraint theory (TCT, or rigidity theory) [1–4] offers an elegant framework to predict the properties of glasses as a function of their composition and structure [5–9]. TCT consists of reducing the complex atomic structure of glasses to a mechanical truss, wherein some nodes (the atoms) are connected to each other via some topological constraints (the chemical bonds) [5]. This level of simplification makes it possible to "separate the wheat from the chaff," that is, to isolate the important role of the connectivity of the atomic network while filtering out other less relevant structural details, which, in many cases, only have a second-order effect on macroscopic properties [6]. In molecular glasses, the relative positions of the atoms are constrained by (i) radial bond-stretching (BS) constraints, which keep the interatomic bonds fixed around the average bond length, and (ii) angular bond-bending (BB) constraints, which define the angular environment around each atom. The state of rigidity of a given glass can then be determined by enumerating the number of BS and BB constraints acting in the atomic network. Based on Maxwell's stability criterion [10], a glass network is defined as flexible (underconstrained), stressed-rigid (overconstrained), or isostatic (optimally constrained) if the number of constraints is lower, higher, or equal to the number of atomic degrees of freedom (i.e., 3 per atom), respectively.

In the original formulation of TCT introduced by Phillips, Gupta, and Thorpe [1,3,4], the constraints enumeration was conducted at zero temperature, wherein all BS and BB constraints are active. Mauro and Gupta subsequently extended TCT to account for finite temperature effects by introducing temperature-dependent constraint theory [11,12]. In this framework, each constraint is associated with a given activation energy for its breakage (ΔF) and, thereby, can be active (at low temperature) or thermally-broken (at high temperature). Based on this idea, the fraction $q(T)$ of a particular type of constraints that is active at a given temperature T can be expressed as:

* Corresponding author.
E-mail address: bauchy@ucla.edu (M. Bauchy).

https://doi.org/10.1016/j.jnoncrysol.2020.120614
Received 5 October 2020; Received in revised form 25 November 2020; Accepted 14 December 2020
Available online 5 January 2021

$$q(T) = \left[1 - \exp\left(-\frac{\Delta F}{kT}\right)\right]^{\nu t_{\text{obs}}} \quad (1)$$

where k is the Boltzmann constant, ν is the vibrational attempt frequency for breaking a constraint, and t_{obs} is the observation time [11]. The temperature-dependence of constraints and the form of Eq. 1 were later confirmed by molecular dynamics simulations [13]. Further, if $\nu t_{\text{obs}} \gg 1$, the fraction of intact constraints can be approximated by a Heaviside step function $H()$:

$$q(T) = H(T_q - T) \quad (2)$$

where T_q is the onset temperature below which a given constraint becomes active.

Importantly, depending on their strength, different types of constraints are associated with varying onset temperature (or varying activation energy for breaking). For instance, inter-polytope angular constraints (e.g., Si–O–Si bonds) have been assumed to break at a lower temperature than intra-polytope constraints (e.g., O–Si–O bonds) [8,11,14], which echoes the fact that, although network-forming polytopes remain fairly rigid themselves, inter-polytope angles exhibit some flexibility [13,15–17]. However, the onset temperatures associated with each particular type of constraint remain fundamentally unknown and are usually considered solely as fitting parameters.

Here, we present a generic approach aiming to predict the onset temperature of topological constraints by means of molecular dynamics (MD) simulations. We illustrate this approach by taking the example of a series of archetypical binary calcium silicate glasses with varying compositions—a family of glass that has important applications as bioactive material or cementing phase [18]. As expected, we find that inter-polytope Si–O–Si BB constraints are associated with a lower onset temperature than intra-polytope O–Si–O BB constraints. The onset temperatures determined by the analysis allow us to describe the compositional dependence of the fictive temperature of the glasses simulated herein.

2. Methods

2.1. Simulation of the glasses

To establish our conclusions, we simulate by classical MD simulations a series of binary $(CaO)_x(SiO_2)_{1-x}$ glasses with varying molar fractions of CaO (x) ranging from 0-to-80%. Each glass is comprised of about 3000 atoms, which are initially randomly placed in a cubic simulation box while ensuring the absence of any unrealistic overlap. Each system is then melted at 3000 K in the canonical (*NVT*) ensemble for 100 ps and, subsequently, in the isothermal-isobaric (*NPT*) ensemble under zero pressure for another 100 ps—which ensures that the simulated melts lose the memory of their initial structure. The equilibrated melts are then cooled down to 300 K in the *NPT* ensemble under zero pressure with a cooling rate of 1 K/ps, before a final equilibration of 100 ps at 300 K [19]. Six independent melt-quench simulations are conducted for each glass composition to estimate statistical uncertainties. For all simulations, we use the Buckingham interatomic forcefield developed by Jakse *et al.* [20,21], which has been shown to offer an improved description of the structure, dynamics, and mechanics of calcium aluminosilicate glasses as compared to alternative forcefields [22–25]. Coulombic interactions are computed with the Ewald summation method, with a convergence criterion of 10^{-5}. Cutoffs of 8 and 12 Å are used for the short-range and Coulombic interactions, respectively. All simulations are conducted with the LAMMPS package [26], with an integration timestep of 1 fs, and using the Nosé–Hoover thermostat [27,28]. More details on the simulations and on the validation of the interatomic forcefield can be found in Ref. [22].

2.2. Fictive temperature

The fictive temperature of each glass is determined based on the method introduced in Ref. [29], which is detailed in the following. The method is based on tracking the evolution of the potential energy of the inherent structure of the simulated systems as a function of temperature during their quenching. In detail, following Section 2.1, we first quench the system from 3000 K down to 300 K with a cooling rate of 1 K/ps in the *NPT* ensemble (under zero pressure). Every 100 ps, we then extract a configuration for further analysis. For each configuration (i.e., at each temperature), we conduct a subsequent run of 80 ps in the *NPT* ensemble while keeping constant the temperature. A total of 16 independent configurations are then extracted from each run (every 5 ps). Each of these configurations is then subjected to a constant-volume energy minimization (using the conjugate gradient algorithm) to compute the potential energy U of its inherent configuration (i.e., the local minimum of energy that is accessible to the system) [19,30]. For illustration purposes, the potential energy of a simulated glass (SiO_2) before and after energy minimization is shown in Fig. 1a. For each initial temperature, we then calculate the average inherent structure energy by averaging over the 16 independent configurations (see Fig. 1b). The fictive temperature of the glass (which is associated with its structural arrest as the temperature decreases) then manifests itself as a break in slope in the U vs. T curve (see Fig. 1c). Specifically, the fictive temperature of each glass is determined by performing two linear regressions of the U vs. T plot in the low- and high-temperature domains—and the fictive temperature T_f is here defined as the temperature at which these two linear functions intersect with each other. By focusing on the inherent structure energy rather than on the instantaneous energy (i.e., at finite temperature) during quenching, this analysis filters out thermal effects and yields a clearer signature of the glass transition (see Refs. [20,29,31–33]). Note that the fictive temperature is not strictly a glass property as it depends on the cooling rate—so that fictive temperatures determined by MD simulations typically far exceed the associated experimental values [19].

2.3. Structural analysis

As a prerequisite for the enumeration of the topological constraints acting in the atomic network of the simulated glasses, we compute the coordination number of each atom. To this end, we first determine the extent of the first coordination shell of each type of atom—which is here defined as the position of the first minimum after the first peak in the partial pair distribution function associated with each element. We then directly enumerate the number of neighbors that are present in the first coordination shell of each atom. This allows us to distinguish the different types of O species that are present in the glass, namely, bridging oxygen (BO, which are connected to two Si atoms), non-bridging oxygen (NBO, which are connected to only one Si atom), and free oxygen (FO, which are not connected to any Si atom). Based on this analysis, we then decompose the total coordination of Ca atoms into the contributions of BO, NBO, and FO.

3. Results

3.1. Coordination numbers

We first focus on the evolution of the coordination number of each atomic species in the atomic network as a function of the glass composition. We note that Si atoms systematically remain 4-fold coordinated, irrespectively of the composition of the glass. Therefore, we focus our attention on O and Ca species.

Fig. 2a shows the fraction of BO, NBO, and FO species as a function of composition. As expected, we find that pure SiO_2 is only comprised of BO atoms. The addition of CaO in the glass then results in the formation of NBO atoms at the expense of BO atoms—which is not surprising since,

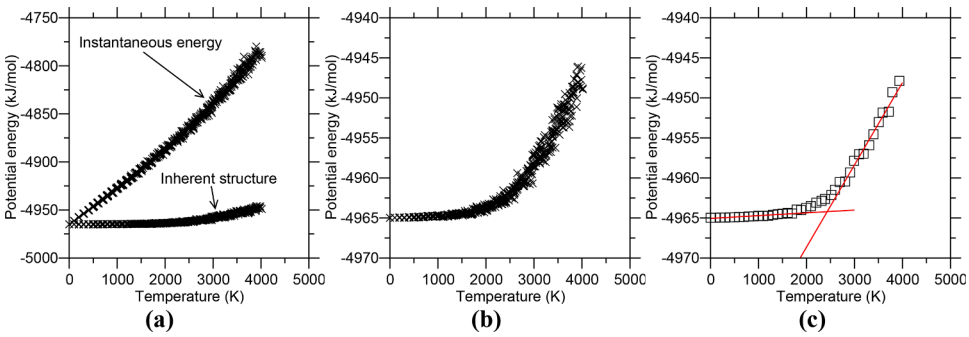

Fig. 1. (a) Instantaneous potential energy (at finite temperature) and potential energy of the inherent structure after energy minimization, (b) potential energy of the inherent structure (zoomed in), and (c) averaged potential energy of the inherent structure (averaged over 16 independent configurations per initial temperature) as a function of the initial temperature for a simulated SiO_2 glass-forming system. The solid lines are some linear fits at low and high temperature. The intersection of these lines yields the glass fictive temperature.

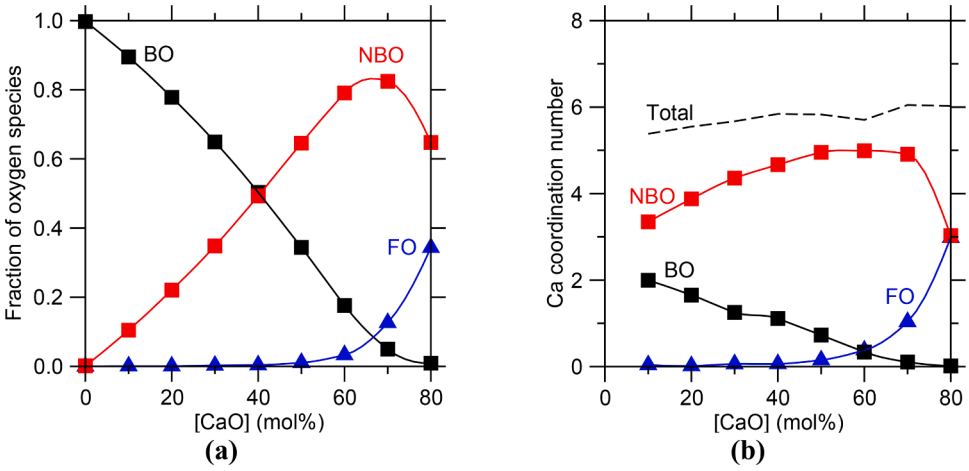

Fig. 2. (a) Fractions of bridging oxygen (BO), non-bridging oxygen (NBO), and free oxygen (FO) in binary calcium silicate glasses as a function of composition. (b) Average BO, NBO, and FO partial coordination numbers of the Ca atoms in calcium silicate glasses as a function of composition. The dashed line indicates the total coordination number of the Ca atoms (i.e., the sum of the partials). In both panels, the solid lines are to guide the eye. In both panels, error bars are smaller than the symbol size.

in this regime, each Ca atom is indeed expected to form two NBO atoms [34]. However, we note that, in Ca-rich glasses, the addition of CaO eventually results in the formation of FO atoms. Although such Ca-rich calcium silicate glasses have not been experimentally studied due to their low glass-forming ability, the existence of such FO species has been suggested in other silicate glasses [35–37]. Here, we find that the fraction of FO atoms starts to notably increase for [CaO] > 60%, which corresponds to the range of compositions wherein the fraction of BO atoms becomes nearly zero. Starting from a fully polymerized network in pure SiO_2 (wherein all O atoms act as BO) and assuming that each Ca atom creates two NBO atoms, one would indeed expect all BO atoms to be consumed at [CaO] = 2/3 (66.7%). At this threshold, the glass network would be solely composed of isolated SiO_4 tetrahedral units, which are connected to each other via some weak O–Ca–O ionic bonds. Starting from this initial structure, any further addition of CaO would indeed result in the formation of FO atoms (i.e., Ca–O–Ca bonds).

Next, we focus on Ca atoms. We first note that the total coordination number of Ca atoms only exhibits a slight increase upon increasing CaO content (Fig. 2b) and, as expected, remains close to 6, irrespectively of the glass composition [38–40]. We then track the contribution of each type of O species to the coordination of Ca atoms. Qualitatively, the evolution of the BO, NBO, and FO partial coordination numbers of Ca atoms follows the trends observed in Fig. 2a—since the addition of CaO in the glass initially tends to increase the average number of NBO atoms that are present in the first coordination shell of Ca atoms, while the contribution of FO atoms eventually increases in Ca-rich glasses. However, we note that the distribution of the partial Ca–O coordination numbers does not fully mimic the populations of the different O species. Specifically, we observe that Ca atoms are preferentially connected to NBO and FO atoms (at the expense of BO atoms). This is not surprising since, in contrast to NBO and FO atoms, the charge of BO atoms is already fully compensated by their two nearest Si neighbors.

3.2. Topological constraints in the glassy state

The structural analysis presented in Section 3.1 allows us to infer the types of topological constraints that are at play in the atomic network of calcium silicate glasses (i.e., at 300 K). We first focus on the 2-body radial BS constraints. Note that each BS constraint is necessarily shared by a cation (i.e., Si or Ca) and an O atom. Here, for simplicity, we fully attribute all BS constraints to the associated cation. As expected, since they have a fixed coordination number of 4, Si atoms create 4 BS constraints with their 4 O neighbors [13]. In contrast, Ca atoms exhibit more variability in their coordination number. On average, Ca atoms tend to create 5-to-6 BS constraints with their O neighbors [41,42]. Next, we focus on the 3-body angular BB constraints. As expected, Si atoms create 5 BB constraints, which keep the O–Si–O angles fixed around their average value of 109° [17]. Note that, although the Si tetrahedron exhibits 6 distinct O–Si–O angles, only 5 of the angles are mutually independent and, hence, are counted as active BB constraints. In addition, BO atoms create 1 BB constraint, which fixes the value of the Si–BO–Si intertetrahedral angle [13]. In contrast to the strong and directional ionic-covalent Si–O bonds, ionic Ca–O bonds are weaker and virtually non-directional. The ionicity of these bonds manifests itself by very broad Si–NBO–Ca and O–Ca–O partial bond angle distributions, even at room temperature [41]. As such, no BB constraint is associated with NBO and Ca atoms.

3.3. Effect of temperature on angular bond-bending constraints

Next, we focus on the effect of temperature on the state of the topological constraints. We first note that Si and Ca atoms maintain their coordination number up to high temperatures (3000 K). This indicates that their associated BS constraints are strong enough to remain intact, even in the supercooled liquid state. Hence, in the following, we focus on

the state of the weaker angular constraints as a function of temperature [43].

To characterize whether a given BB constraint is active or not at a given temperature, we follow the approach introduced in Ref. [13]. This approach is based on the idea that, rather than directly attempting to identify constraints, it is more convenient to indirectly infer their existence by analyzing the interatomic motion (or absence thereof)—in the same fashion as one can calculate the gravitational force acting on a projectile by analyzing its parabolic trajectory. In the case of atomic networks, the absence of any substantial relative motion between atoms suggests the existence of an underlying constraint, whereas large interatomic motion is indicative of the absence of any underlying constraint.

In detail, for each central atom (i.e., Si or BO), we first identify the N nearest neighbors (here, we use $N = 6$ to ensure that all potential nearest neighbors are accounted for). These N nearest neighbors form $N(N-1)/2$ distinct angles around the central atom 0 (i.e., angles 102, 103, 104, 105, 106, 203, etc.). Note that the N nearest neighbors can change over time and are redefined at each step based on their distance from the central atom. We then track the value of each individual angle over time. This allows us to compute the (i) average θ and (ii) standard deviation σ_θ of each angle. The value of σ_θ corresponds to the angular excursion (in °) of each angle formed around the central atom. Based on these values, we then calculate the relative angular excursion of each angle as σ_θ/θ (in %). This analysis allows us to indirectly infer the existence of individual BB constraints. Indeed, low relative angular excursion values indicate the existence of an underlying BB constraint (which is maintaining the angle fixed around its average value), whereas, in contrast, large relative angular excursion values denote the absence of any underlying BB constraint.

To assess the effect of temperature on the state of the BB constraints, we repeat this analysis at different temperatures. In detail, starting from the glass configurations relaxed at 300 K, we gradually increase the temperature by increments of 100 K. At each temperature step, the system is first subjected to a linear increase in temperature (with a total increase of 100 K) over a duration of 10 ps in the *NPT* ensemble. After heating, the system is then further subjected to a 100 ps run at constant temperature in the *NVT* ensemble. During this phase, 100 configurations are extracted (every 1 ps) and used to calculate the relative angular excursion σ_θ/θ of each interatomic angle in the atomic network.

In the following, we illustrate this method by focusing on the case of the $(CaO)_{50}(SiO_2)_{50}$ glass, noting that similar relative angular excursions are obtained for the other glass compositions. Fig. 3 shows the distributions of the relative angular excursions σ_θ/θ associated with Si and bridging O (BO) atoms (i.e., 4 O–Si–O angles around each Si atom and 1 Si–BO–Si angle around each BO). In general, we find that the relative angular excursions around Si atoms are lower than those around BO atoms—in agreement with the fact that intra-polytope (inside the SiO_4 polytopes) BB constraints are expected to be stronger than inter-polytope (in between the SiO_4 polytopes) BB constraints [11,13]. We then note that both of these distributions gradually shift toward larger relative angular excursions as temperature increases. This signals the fact that, upon increasing temperature, BB constraints become less active since their ability to maintain the angles fixed around their average value decreases.

We observe some notable differences in the behaviors of Si and BO angular BB constraints upon increasing temperature. First, in the case of the O–Si–O BB constraints (Fig. 3a), we find that the maximum position of the distribution only shows a moderate shift toward larger relative angular excursion upon increasing temperature. However, a long tail expanding toward very large angular excursions gradually forms upon increasing temperature. This signals that, as temperature increases, a large number of angular BB constraints remain fairly unaffected, while, in turn, a fraction of the BB constraints break in a dramatic fashion (as evidenced by a very large angular excursion). Indeed, it has previously been shown that, around each Si atom, the BB constraints involving the fourth O neighbor (i.e., angles 104, 204, and 304) are the first to break, while the other BB constraints (i.e., angles 102, 103, and 203) remain active even until very high temperature [13]. In contrast, Si–BO–Si BB constraints (Fig. 3b) exhibit a different behavior upon increasing temperature—as the relative angular excursion distributions gradually shift "in-block" toward larger values upon increasing temperature. This suggests that these constraints collectively break as temperature increases.

3.4. Onset temperature of angular bond-bending constraints

We then estimate the onset temperature associated with these BB constraints by plotting the average relative angular excursion associated with Si and BO atoms as a function of temperature (see Fig. 4). Overall, we note that the average relative angular excursions of Si and BO atoms exhibit a rough bilinear behavior, that is, they are fairly constant at low temperature, and then tend to increase linearly with increasing temperature. We do not observe any discontinuity in the average relative angular excursions that would clearly signal that the onset temperature has been reached. Rather, here, we use 7% as the critical relative angular excursion that discriminates active from thermally-broken BB constraints. This value is based on previous studies that suggested that this threshold properly separates intact from broken constraints [13,41]. The threshold value is also fairly close to the Lindemann criterion, which provides as estimation of the magnitude of atomic vibrations that is required to induce melting [44]. Based on this, we estimate the onset

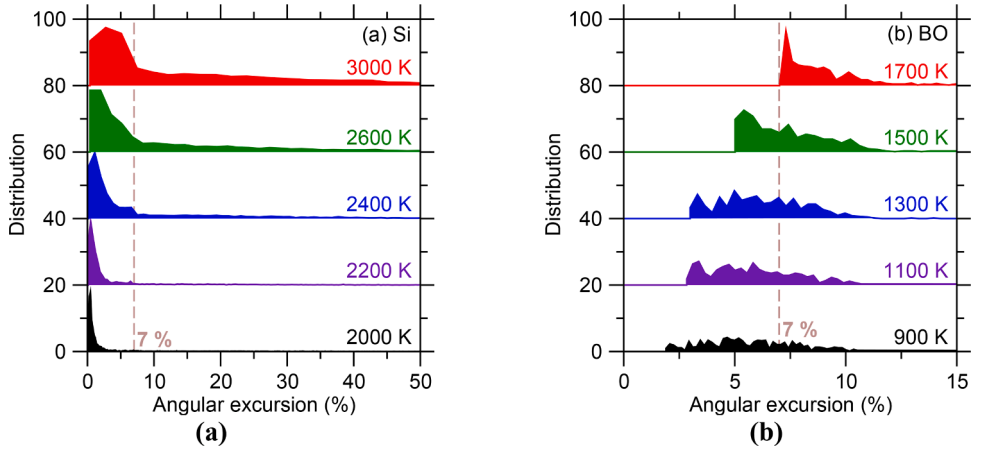

Fig. 3. Distributions of the relative angular excursions of the angles forming around (a) Si atoms (i.e., 4 O–Si–O angles) and (b) bridging oxygen (BO) atoms (i.e., 1 Si–BO–Si angle) at several increasing temperatures in a $(CaO)_{50}(SiO_2)_{50}$ glass.

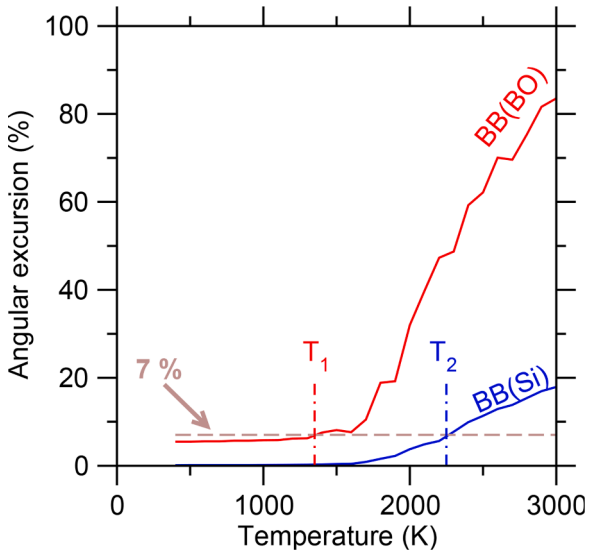

Fig. 4. Average relative angular excursions associated with the bond-bending (BB) constraints created around Si and bridging oxygen (BO) atoms, respectively (i.e., O–Si-O and Si–BO–Si) in a $(CaO)_{50}(SiO_2)_{50}$ glass, as a function of temperature. The horizontal line indicates the relative angular excursion threshold (7%), separating intact (< 7%) from thermally-broken (> 7%) constraints.

temperature of each type of constraint as the temperature at which the average relative angular excursion crosses the threshold value of 7%. This analysis yields notably different onset temperature values for Si–BO–Si and O–Si–O BB constraints, namely, $T_1 = 1350$ K and $T_2 = 2250$ K—although there is some uncertainty in the exact values of these onset temperature (especially in T_1), considering the fluctuations in the σ_θ/θ vs. T curves (see Fig. 4). Nevertheless, these values clearly echo the fact that O–Si–O BB constraints are stronger than Si–BO–Si constraints (namely, they are associated with higher activation energy) and, hence, can sustain higher temperatures before breaking.

It is worth noting that, at this point, this analysis yields the onset temperature that is associated with the observation timescale of the MD simulations (i.e., 100 ps at each step of temperature), which is vastly different from the observation timescale of experimentally produced glasses (i.e., around 100 s). As such, the onset temperatures offered by this analysis are not expected to be directly comparable to experiments (see Discussion Section).

3.5. Effect of the onset temperatures on fictive temperature

We then assess how the two onset temperatures T_1 and T_2 determined in Fig. 4 control the fictive temperature of the simulated glasses. To this end, we adopt the temperature-dependent constraint approach introduced by Mauro and Gupta [11,12], which establishes that the fictive temperature T_f of a given glass composition x can be expressed as:

$$\frac{T_f(x)}{T_f(x_{ref})} = \frac{f(T_f(x_{ref}), x_{ref})}{f(T_f(x), x)} = \frac{3 - n_c(T_f(x_{ref}), x_{ref})}{3 - n_c(T_f(x), x)} \quad (3)$$

where 3 is the initial number of degrees of freedom per atom (in three-dimensional networks), x_{ref} is an arbitrary reference composition associated with a known fictive temperature $T_f(\underline{x}_{ref})$, $n_c(T, x)$ is the total number of constraints per atom that are active at the temperature T for the glass composition x, and $f(T, x) = 3 - n_c(T, x)$ is the number of floppy modes per atom (i.e., the remaining number of degrees of freedom that are not balanced by a topological constraint) [5]. As such, Eq. 3 can be used to predict the compositional evolution of the fictive temperature T_f based on the knowledge of (i) the number of constraints per atom that are active at a given temperature and (ii) the fictive temperature of a reference glass composition. Note that Eq. 3 was initially derived to predict the glass transition temperature T_g (that is, the temperature at which the viscosity is equal to 10^{12} Pa•s, corresponding to a relaxation time of about 100 s) [11]. However, the same equation can be used to predict the fictive temperature, which, here, is the temperature at which the glass relaxation time becomes equivalent to the simulation observation time.

It is worth noting that Eq. 3 is recursive, since predicting T_f requires the knowledge of n_c at this temperature, which itself depends on T_f (since some constraints can form or break depending on the temperature). As such, Eq. 3 can be solved by (i) determining which constraints are active at the temperature $T_f(\underline{x}_{ref})$, i.e., the fictive temperature of the reference glass composition, (ii) determining the number of constraints per atom $n_c(x)$ for the other glass compositions x while assuming that the same types of constraints remain active, (iii) calculating T_f based on Eq. 3, and, finally, (iv) ensuring that the calculated value of T_f does not deviate from $T_f(\underline{x}_{ref})$ enough to break (if T_f increases too much) or form (if T_f decreases too much) another type of constraint.

Interestingly, if the fictive temperature T_f becomes equal to (or is about to exceed) one of the onset temperatures (below which a given type of constraint forms), T_f tends to exhibit a local plateau as a function of the composition x and becomes equal to the onset temperature. For instance, in the present case of calcium silicate glasses, the number of constraints per atom tends to increase with decreasing x (since the connectivity of the glass increases). Upon decreasing x, if the number of constraints increases so much that T_f exceeds the onset temperature of a given type of constraint, this constraint will break. As a result, the breaking of these constraints will reduce the number of constraints, which, in turn, will decrease T_f. This would cause T_f to become lower that the onset temperature, so that the associated constraints would form again. Overall, due to this retroactive mechanism, the fictive temperature T_f will remain equal to the constraint onset temperature over a window of glass compositions x. In this case, T_f will remain equal to the onset temperature until the composition x decreases enough for the number of constraints to become so high (even though certain constraints are thermally-broken) that the value of T_f calculated by Eq. 3 becomes higher than the onset temperature. Similarly, T_f is also expected to exhibit a plateau if, as x increases, the number of constraints decreases so much that T_f becomes lower than the onset temperature of a given type of constraint (so that, at this temperature, some new constraints would form). This interesting behavior is all the more important herein as it allows us to *a posteriori* confirm the values of the onset temperatures identified in Fig. 4 based on the evolution of $T_f(x)$.

Based on this approach, we attempt to predict the compositional dependence of fictive temperature in the present calcium silicate glasses based on their topology. To this end, we first calculate the number of constraints per atom n_c as a function of composition within three different ranges of temperature, namely, (i) $T < T_1$, wherein all constraints are active, (ii) $T_1 < T < T_2$, wherein Si–O–Si BB constraints are broken, and (iii) $T > T_2$, wherein both Si–O–Si and O–Si–O BB constraints are broken (Fig. 5a). As expected, we find that the number of constraints tends to decrease upon increasing temperature (since increasing temperature results in the breaking of constraints). At low temperature ($T < T_1$, i.e., in the glassy state), the number of constraints per atom notably decreases upon increasing [CaO]. This results from the fact that the addition of Ca cations greatly reduces the number of angular BB constraints (since Ca cations consume BOs and replace directional Si–O bonds by non-directional Ca–O bonds). However, this trend is reversed at elevated temperature ($T > T_2$, i.e., in the liquid state). Indeed, in this range of temperature, all BB constraints are broken, so that the addition of Ca cations actually results in an increase in the number of BS constraints (since 4-fold coordinated Si are replaced by 6-fold coordinated Ca atoms). This illustrates that compositional trends in the topology of liquids (wherein radial BS constraints are predominant) may not always follow those observed in the glassy state (wherein both radial BS and angular BB constraints are at play).

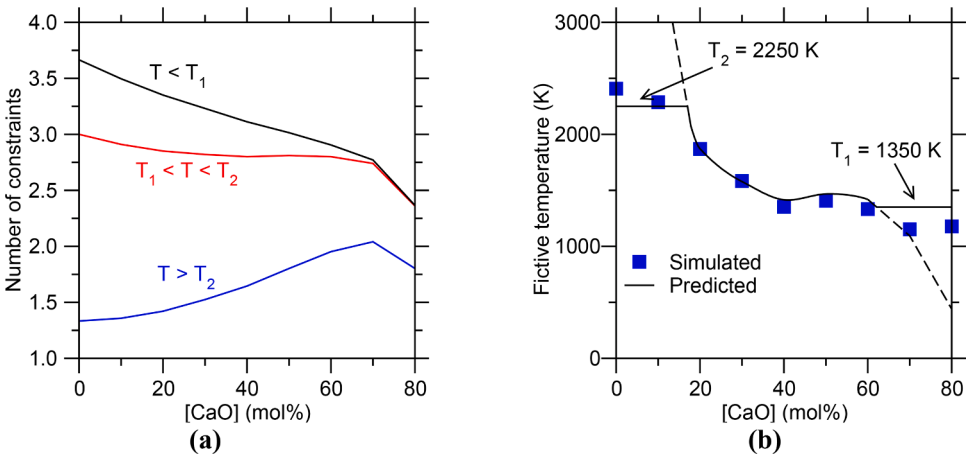

Fig. 5. (a) Number of constraints per atom within different ranges of temperatures as a function of composition. (b) Fictive temperature T_f as a function of composition. The error bars are smaller than the symbol size. The solid line shows the predicted T_f values using Eq. 3, while the square symbols correspond to the T_f values computed by MD simulations. The dashed lines indicate the predicted evolution of T_f if O–Si–O constraints did not break at the onset temperature $T_2 = 2250$ K and if Si–O–Si constraints did not form at the onset temperature $T_1 = 1350$ K.

Based on the number of constraints per atoms n_c presented in Fig. 5a, we then attempt to predict the evolution of the fictive temperature T_f of the calcium silicate glasses using Eq. 3. To this end, we adopt as reference composition $x_{ref} = 20\%$. The choice of this reference is motivated by the fact that, for this composition, the fictive temperature is $T_f(x_{ref}) \approx 1800$ K, which is conveniently located in between the onset temperatures T_1 and T_2 identified in Fig. 4 (so that, at this temperature, O–Si–O constraints are active but Si–O–Si constraints are thermally-broken). As such, this composition offers an ideal reference point to determine the onset temperatures T_1 (which is likely to result in a plateau in T_f upon decreasing n_c) and T_2 (which is likely to result in a plateau in T_f upon increasing n_c).

Fig. 5b shows the fictive temperature that is predicted by Eq. 3 as a function of composition. As expected, we find that the predicted fictive temperature decreases upon increasing [CaO], which echoes the fact that, in the considered initial range of temperature ($T_1 < T < T_2$), the number of constraints per atom decreases upon increasing [CaO]. Importantly, we find that, on the one hand, the predicted fictive temperature quickly increases toward infinity in Ca-poor glasses (see the dashed line on the left in Fig. 5b). This is a consequence of the fact that, in the considered initial range of temperature ($T_1 < T < T_2$), the number of constraints per atom n_c converges toward 3 for [CaO] = 0 (in agreement with the fact that pure silica is associated with an isostatic network [5]). Indeed, following Eq. 3, $n_c = 3$ would result in an infinite value for T_f. At [CaO] = 17%, the predicted fictive temperature eventually reaches T_2, so that, at this point, angular O–Si–O BB constraints break. As mentioned above, this results in a plateau in T_f for [CaO] < 17%. On the other hand, we find that the predicted fictive temperature eventually drops toward low values in Ca-rich glasses (see right dashed line in Fig. 5b). This is a result of the fact that, in the considered initial range of temperature ($T_1 < T < T_2$), the number of constraints per atom n_c tends to quickly decrease in Ca-rich glasses (eventually becoming lower than 2.5). At [CaO] = 61%, the predicted fictive temperature reaches T_1, so that, at this point, angular Si–O–Si BB constraints become active. This results in a plateau in T_f for [CaO] > 61%.

Overall, we find that the fictive temperature that is predicted by the present model exhibits a fairly good match with the simulated data over the entire range of glass compositions (see Fig. 5b). Notably, the plateaus observed in the compositional dependence of the predicted fictive temperature are well supported by the MD data, both in Ca-poor glasses (wherein T_f plateaus at T_2) and Ca-rich glasses (wherein T_f plateaus at T_1). Note that, since MD simulations are associated with very high cooling rates, they offer largely overestimated values of T_f as compared to experimental data [19]. For instance, experimental fictive temperature values for [CaO] = 50% are found to be around 1050-to-1060 K [45, 46], which is notably lower than the simulated value obtained herein (1406 K). The effect of the cooling rate is further discussed in the Discussion section. Nevertheless, the overall harmony between predicted and simulated T_f values demonstrated in Fig. 5b *a posteriori* supports the validity of the onset temperatures T_1 and T_2 identified in Fig. 4.

4. Discussion

In this section, we discuss how the present simulation results can be translated to experimental glasses. Indeed, no matter how accurate the interatomic forcefield used in simulations may be, MD simulations can only access very short timescales (e.g., a few nanoseconds) as compared to experimental timescales (e.g., hundreds of seconds). Due to this difference in timescale, the cooling rate used in MD simulations (typically 1 K/ps) is orders of magnitude larger than typical experimental conditions of glass formation (typically 1 K/s) [19]. As a result, since the observation time accessible to MD simulations is notably smaller than that accessible to experiments, simulated melts typically exhibit a dynamical arrest (i.e., when their relaxation time equal the observation time) at more elevated temperature than their experimental counterparts [47, 48]—so that simulated glasses typically exhibit larger fictive temperature than experimental glasses. This limited timescale is also likely to affect the onset temperature of topological constraints, since, at a given temperature, a constraint that appears to be active when observed during a short time may appear to be broken when observed for a longer duration.

In the framework of temperature-dependent topological constraint theory, the influence of timescale is encoded in the νt_{obs} term in Eq. 1. Unfortunately, this term has thus far mostly been treated as a fitting parameter, and its dependence on the cooling rate remains unclear [8]. Here, as an attempt to convert the onset temperatures obtained herein (i.e., associated with the limited timescale of MD simulations) into onset temperatures that are applicable to experimental timescales, we adopt the following approach. First, we track the fraction of active BB constraints as a function of temperature $q(T)$, wherein active constraints are defined as those that are associated with a relative angular excursion that is lower than 7% (based on the distributions shown in Fig. 3). Then, we fit these data with Eq. 1, which yields the parameters ΔF and νt_{obs}. Based on the value of ΔF identified by MD, we finally estimate the onset temperature associated with the experimental timescale by adjusting (increasing) the value of t_{obs} (see below).

The obtained $q(T)$ data are shown in Fig. 6, both for Si- and BO-centered BB constraints. We find that the data can be well fitted by Eq. 1 (see Fig. 6), which offers confidence in the temperature-dependent topological constraint framework. By fitting, we first find $\Delta F = 0.83$ and 0.38 eV for Si- and BO-centered BB constraints, respectively. These values match (in terms of order of magnitude) previous values that were obtained in the case of a simulated sodium silicate glass (0.89 eV) [13].

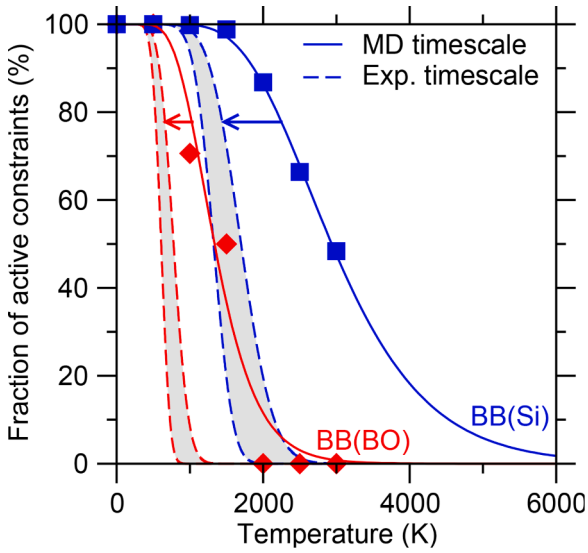

Fig. 6. Fraction of active bond-bending (BB) constraints around Si and bridging oxygen (BO) atoms in a $(CaO)_{50}(SiO_2)_{50}$ glass as a function of temperature. The symbols show the values computed by molecular dynamics (MD) simulations. MD data are fitted with Eq. 1 (solid lines) to get the activation energy ΔF for breaking a constraint. MD data are then extrapolated toward experimental (Exp.) timescales based on Eq. 1 (grey area surrounded by dashed lines). The extrapolation is conducted by using the same ΔF value (determined by MD), but extended observation time (using νt_{obs} = 200-to-1000).

These values also echo the fact that intra-polytope O–Si–O BB constraints are expected to be stronger than inter-polytope Si–BO–Si BB constraints [15]. Then, by fitting, we find νt_{obs} = 18.0 and 18.6 for Si- and BO-centered BB constraints, respectively. The fact that these two values are comparable to each other is consistent with the fact that (i) the vibrational attempt frequencies ν associated with both constraints are expected to be fairly similar and (ii) the observation time t_{obs} solely depends on the timescale of the MD simulation (here, the heating rate). Moreover, these values are fairly comparable with that obtained in the case of a sodium silicate glass (34.3, as obtained for the Si–O–Si BB constraint) [13].

By using the MD-derived activation energy ΔF associated with each constraint, it now becomes possible to estimate the fraction of active constraints $q(T)$ as a function of the parameter νt_{obs} based on Eq. 1. Since the relationship between cooling rate and νt_{obs} is unclear, we simply explore the effect of increasing νt_{obs} (i.e., increasing the observation time). To this end, we consider the range of values νt_{obs} = 200-to-1000, which was previously determined based on experimental fragility data for phosphate and borate glasses [11,49]. Onset temperatures associated with experimental timescales are then defined as the temperature at which $q(T) = 0.5$. Fig. 6 shows the predicted $q(T)$ functions, as calculated by assuming νt_{obs} = 200-to-1000. It is worth noting that, as νt_{obs} increases, the $q(T)$ function gradually converges toward a step function [11]. As a result, the influence of the νt_{obs} term on the onset temperature continuously reduces upon increasing t_{obs}. Indeed, we find that, despite the large range of νt_{obs} values considered herein (i.e., 200-to-1000), the calculated $q(T)$ temperatures exhibit a fairly limited dependence on νt_{obs} (see the gray areas in Fig. 6). Based on this analysis, we find that the onset temperature associated with Si–BO–Si constraints is within 610-to-780 K. This range of values exhibits a very good match with experimental onset temperatures observed in silica (810 K [50,51]) and silicate glasses (720-to-770 K [14]). Similarly, we find that the onset temperature associated with stronger O–Si–O constraints is within 1320-to-1700 K. Although this range of temperature prevents us from being fully conclusive, these values are in agreement with onset temperatures observed in silica (1600 K [50,51]) and silicate glasses (1425 K [52,53]).

5. Conclusions

Overall, the results presented herein offer a generic approach to estimate the onset temperature associated with different topological constraints based on molecular dynamics simulations. Although onset temperatures are timescale-dependent (and, hence, cooling-rate-dependent), the onset temperature values derived by molecular dynamics can be rescaled so as to be consistent with experimental timescales. Importantly, we find that the onset temperatures associated with inter- and intra-polytope angular constraints play a critical role in governing the glass fictive temperature (or glass transition temperature if the observation time is large enough). Indeed, we find that the onset temperatures associated with Si–BO–Si and O–Si–O constraints impose a lower- and upper-bound plateau on the fictive temperature, respectively. This suggests that the existence of such plateaus (wherein the glass transition remains constant upon varying composition) is indicative of the thermal breaking of a topological constraint.

The knowledge of the onset temperature associated with each type of constraint is key to predict the glass transition temperature of glass-forming systems as a function of their composition [11]. More generally, in addition to providing the onset temperature, the present approach also offers a direct estimation of the fraction $q(T)$ of active constraints as a function of temperature. Indeed, although, for the sake of simplicity, analytical topological models are often based on the assumption that all the constraints of a given type instantly break when their onset temperature is reached, the knowledge of the fraction $q(T)$ of active constraints as a function of temperature is important to determine the rate at which constraints break upon increasing temperature, which must otherwise be treated as a fitting parameter. In turn, the rate at which constraints break upon heating is key to predict melt fragility or the temperature dependence of glass stiffness (wherein treating $q(T)$ as a step function is insufficient) [11,51]. We envision that the temperature-dependence of topological constraints offers a promising pathway to decipher how the properties of glasses are encoded in those of their supercooled liquids parents, and vice versa [54–56].

CRediT authorship contribution statement

Yushu Hu: Conceptualization, Methodology, Investigation, Writing - original draft, Writing - review & editing. **Zegao Liu: . Kai Yang:** Methodology, Software, Validation. **N M Anoop Krishnan:** Writing - review & editing, Supervision. **Morten M. Smedskjaer:** Writing - review & editing, Supervision. **Gaurav Sant:** Conceptualization, Resources, Writing - review & editing, Funding acquisition. **Mathieu Bauchy:** Conceptualization, Writing - review & editing, Supervision, Project administration, Funding acquisition.

Declaration of Competing Interest

The authors declare that they have no known competing financial interests or personal relationships that could have appeared to influence the work reported in this paper.

Acknowledgments

This work was supported by the National Science Foundation (under Grants No. CMMI-1762292, DMR-1928538, and DMR-1944510) and the Federal Highway Administration (Grant #: 693JJ31950021). N.M.A.K. also acknowledges some financial support provided by the Department of Science and Technology, India under the INSPIRE faculty scheme (DST/INSPIRE/04/2016/002774) and DST SERB Early Career Award (ECR/2018/002228).

References

[1] J.C. Phillips, Topology of covalent non-crystalline solids .1. Short-range order in chalcogenide alloys, J. Non-Cryst. Solids. 34 (1979) 153–181, https://doi.org/10.1016/0022-3093(79)90033-4.

[2] J.C. Phillips, Topology of covalent non-crystalline solids II: medium-range order in chalcogenide alloys and As-Si-Ge, J. Non-Cryst. Solids 43 (1981) 37–77, https://doi.org/10.1016/0022-3093(81)90172-1.

[3] P.K. Gupta, A.R. Cooper, Topologically disordered networks of rigid polytopes, J. Non-Cryst. Solids 123 (1990) 14–21, https://doi.org/10.1016/0022-3093(90)90768-H.

[4] M.F. Thorpe, Continuous deformations in random networks, J. Non-Cryst. Solids. 57 (1983) 355–370, https://doi.org/10.1016/0022-3093(83)90424-6.

[5] M. Bauchy, Topological Constraint Theory and Rigidity of Glasses, 21st Century Nanoscience – A Handbook., 2019, https://doi.org/10.1201/9780367333003-13.

[6] J.C. Mauro, Topological constraint theory of glass, Am. Ceram. Soc. Bull. 90 (2011) 31–37.

[7] M. Bauchy, Deciphering the atomic genome of glasses by topological constraint theory and molecular dynamics: a review, Comput. Mater. Sci. 159 (2019) 95–102, https://doi.org/10.1016/j.commatsci.2018.12.004.

[8] M.M. Smedskjaer, J.C. Mauro, S. Sen, Y. Yue, Quantitative design of glassy materials using temperature-dependent constraint theory, Chem. Mat. 22 (2010) 5358–5365, https://doi.org/10.1021/cm1016799.

[9] M. Micoulaut, Y. Yue, Material functionalities from molecular rigidity: Maxwell's modern legacy, MRS Bull.. 42 (2017) 18–22, https://doi.org/10.1557/mrs.2016.298.

[10] J.C. Maxwell, L. On the calculation of the equilibrium and stiffness of frames, Philos. Mag. Ser. 4 (27) (1864) 294–299, https://doi.org/10.1080/14786446408643668.

[11] P.K. Gupta, J.C. Mauro, Composition dependence of glass transition temperature and fragility. I. A topological model incorporating temperature-dependent constraints, J. Chem. Phys. 130 (2009), https://doi.org/10.1063/1.3077168, 094503-094503–8.

[12] J.C. Mauro, P.K. Gupta, R.J. Loucks, Composition dependence of glass transition temperature and fragility. II. A topological model of alkali borate liquids, J. Chem. Phys. 130 (2009), 234503, https://doi.org/10.1063/1.3152432.

[13] M. Bauchy, M. Micoulaut, Atomic scale foundation of temperature-dependent bonding constraints in network glasses and liquids, J. Non Cryst. Solids 357 (2011) 2530–2537, https://doi.org/10.1016/j.jnoncrysol.2011.03.017.

[14] C.J. Wilkinson, A.R. Potter, R.S. Welch, C. Bragatto, Q. Zheng, M. Bauchy, M. Affatigato, S.A. Feller, J.C. Mauro, Topological origins of the mixed alkali effect in glass, J. Phys. Chem. B. 123 (2019) 7482–7489, https://doi.org/10.1021/acs.jpcb.9b06512.

[15] M. Wang, B. Wang, T.K. Bechgaard, J.C. Mauro, S.J. Rzoska, M. Bockowski, M. M. Smedskjaer, M. Bauchy, Crucial effect of angular flexibility on the fracture toughness and nano-ductility of aluminosilicate glasses, J. Non Cryst. Solids 454 (2016) 46–51, https://doi.org/10.1016/j.jnoncrysol.2016.10.020.

[16] M. Zhang, P. Boolchand, The central role of broken bond-bending constraints in promoting glass formation in the oxides, Science 266 (1994) 1355–1357, https://doi.org/10.1126/science.266.5189.1355.

[17] M. Bauchy, M. Micoulaut, M. Celino, S.L. Roux, M. Boero, C. Massobrio, Angular rigidity in tetrahedral network glasses with changing composition, Phys. Rev. B. 84 (2011), 054201, https://doi.org/10.1103/PhysRevB.84.054201.

[18] T.F. Watson, A.R. Atmeh, S. Sajini, R.J. Cook, F. Festy, Present and future of glass-ionomers and calcium-silicate cements as bioactive materials in dentistry: biophotonics-based interfacial analyses in health and disease, Dent. Mater. 30 (2014) 50–61, https://doi.org/10.1016/j.dental.2013.08.202.

[19] X. Li, W. Song, K. Yang, N.M.A. Krishnan, B. Wang, M.M. Smedskjaer, J.C. Mauro, G. Sant, M. Balonis, M. Bauchy, Cooling rate effects in sodium silicate glasses: bridging the gap between molecular dynamics simulations and experiments, J. Chem. Phys. 147 (2017), 074501, https://doi.org/10.1063/1.4998611.

[20] M. Bouhadja, N. Jakse, A. Pasturel, Striking role of non-bridging oxygen on glass transition temperature of calcium aluminosilicate glass-formers, J. Chem. Phys. 140 (2014), 234507, https://doi.org/10.1063/1.4882283.

[21] M. Bouhadja, N. Jakse, A. Pasturel, Structural and dynamic properties of calcium aluminosilicate melts: a molecular dynamics study, J. Chem. Phys. 138 (2013), 224510, https://doi.org/10.1063/1.4809523.

[22] M. Bauchy, Structural, vibrational, and elastic properties of a calcium aluminosilicate glass from molecular dynamics simulations: the role of the potential, J. Chem. Phys. 141 (2014), 024507, https://doi.org/10.1063/1.4886421.

[23] B. Wang, Y. Yu, Y.J. Lee, M. Bauchy, Intrinsic nano-ductility of glasses: the critical role of composition, Front. Mater. 2 (2015) 11, https://doi.org/10.3389/fmats.2015.00011.

[24] B. Wang, Y. Yu, M. Wang, J.C. Mauro, M. Bauchy, Nanoductility in silicate glasses is driven by topological heterogeneity, Phys. Rev. B. 93 (2016), 064202, https://doi.org/10.1103/PhysRevB.93.064202.

[25] M.M. Smedskjaer, M. Bauchy, J.C. Mauro, S.J. Rzoska, M. Bockowski, Unique effects of thermal and pressure histories on glass hardness: Structural and topological origin, J. Chem. Phys. 143 (2015), 164505, https://doi.org/10.1063/1.4934540.

[26] S. Plimpton, Fast parallel algorithms for short-range molecular dynamics, J. Comput. Phys. 117 (1995) 1–19.

[27] S. Nosé, A molecular dynamics method for simulations in the canonical ensemble, Mol. Phys. 52 (1984) 255–268, https://doi.org/10.1080/00268978400101201.

[28] W.G. Hoover, Canonical dynamics: equilibrium phase-space distributions, Phys. Rev. A. 31 (1985) 1695–1697, https://doi.org/10.1103/PhysRevA.31.1695.

[29] Z. Liu, Y. Hu, X. Li, W. Song, S. Goyal, M. Micoulaut, M. Bauchy, Glass relaxation and hysteresis of the glass transition by molecular dynamics simulations, Phys. Rev. B. 98 (2018), 104205, https://doi.org/10.1103/PhysRevB.98.104205.

[30] N.M.A. Krishnan, B. Wang, Y. Yu, Y. Le Pape, G. Sant, M. Bauchy, Enthalpy landscape dictates the irradiation-induced disordering of quartz, Phys. Rev. X. 7 (2017), 031019, https://doi.org/10.1103/PhysRevX.7.031019.

[31] S. Urata, An efficient computational procedure to obtain a more stable glass structure, J. Chem. Phys. 151 (2019), 224502, https://doi.org/10.1063/1.5133413.

[32] M. Bouhadja, N. Jakse, A. Pasturel, Stokes–Einstein violation and fragility in calcium aluminosilicate glass formers: a molecular dynamics study, Mol. Simul. 40 (2014) 251–259, https://doi.org/10.1080/08927022.2013.840893.

[33] A. Atila, E.M. Ghardi, A. Hasnaoui, S. Ouaskit, Alumina effect on the structure and properties of calcium aluminosilicate in the percalcic region: a molecular dynamics investigation, J. Non Cryst. Solids 525 (2019), 119470, https://doi.org/10.1016/j.jnoncrysol.2019.119470.

[34] A.K. Varshneya, Fundamentals of Inorganic Glasses, Academic Press Inc, 1993.

[35] H.W. Nesbitt, G.M. Bancroft, G.S. Henderson, R. Ho, K.N. Dalby, Y. Huang, Z. Yan, Bridging, non-bridging and free (O2–) oxygen in Na2O-SiO2 glasses: an X-ray Photoelectron Spectroscopic (XPS) and Nuclear Magnetic Resonance (NMR) study, J. Non Cryst. Solids 357 (2011) 170–180, https://doi.org/10.1016/j.jnoncrysol.2010.09.031.

[36] H. Wayne Nesbitt, G.S. Henderson, G. Michael Bancroft, R. Sawyer, R.A. Secco, Bridging oxygen speciation and free oxygen (O2−) in K-silicate glasses: implications for spectroscopic studies and glass structure, Chem. Geol. 461 (2017) 13–22, https://doi.org/10.1016/j.chemgeo.2016.11.026.

[37] H.W. Nesbitt, G.M. Bancroft, G.S. Henderson, R. Sawyer, R.A. Secco, Direct and indirect evidence for free oxygen (O2−) in MO-silicate glasses and melts (M = Mg, Ca, Pb), Am. Mineral. 100 (2015) 2566–2578, https://doi.org/10.2138/am-2015-5336.

[38] L. Cormier, D.R. Neuville, G. Calas, Structure and properties of low-silica calcium aluminosilicate glasses, J. Non Cryst. Solids 274 (2000) 110–114, https://doi.org/10.1016/S0022-3093(00)00209-X.

[39] D.A. Dutt, P.L. Higby, D.L. Griscom, A structural model for low silica content calcium aluminosilicate glasses, Phys. Chem. Glasses 33 (1992) 51–55.

[40] P.H. Gaskell, M.C. Eckersley, A.C. Barnes, P. Chieux, Medium-range order in the cation distribution of a calcium silicate glass, Nature 350 (1991) 675–677, https://doi.org/10.1038/350675a0.

[41] M. Bauchy, M.J. Abdolhosseini Qomi, C. Bichara, F.-J. Ulm, R.J.-M. Pellenq, Nanoscale structure of cement: viewpoint of rigidity theory, J. Phys. Chem. C. 118 (2014) 12485–12493, https://doi.org/10.1021/jp502550z.

[42] S. Gin, M. Wang, N. Bisbrouck, M. Taron, X. Lu, L. Deng, F. Angeli, T. Charpentier, J.-M. Delaye, J. Du, M. Bauchy, Can a simple topological-constraints-based model predict the initial dissolution rate of borosilicate and aluminosilicate glasses? Npj Mater. Degrad. 4 (2020) 1–10, https://doi.org/10.1038/s41529-020-0111-4.

[43] M. Bauchy, M.J.A. Qomi, C. Bichara, F.-J. Ulm, R.J.-M. Pellenq, Rigidity transition in materials: hardness is driven by weak atomic constraints, Phys. Rev. Lett. 114 (2015), 125502, https://doi.org/10.1103/PhysRevLett.114.125502.

[44] F.A. Lindemann, Ueber die berechnung molekularer eigenfrequenzen, Phys. Z. 11 (1910) 609–612.

[45] H. Jabraoui, M. Malki, A. Hasnaoui, M. Badawi, S. Ouaskit, S. Lebègue, Y. Vaills, Thermodynamic and structural properties of binary calcium silicate glasses: insights from molecular dynamics, Phys. Chem. Chem. Phys. 19 (2017) 19083–19093, https://doi.org/10.1039/C7CP03397D.

[46] M. Micoulaut, M. Malki, P. Simon, A. Canizares, On the rigid to floppy transitions in calcium silicate glasses from Raman scattering and cluster constraint analysis, Philos. Mag. 85 (2005) 3357–3378, https://doi.org/10.1080/14786430500157029.

[47] J. Du, Challenges in molecular dynamics simulations of multicomponent oxide glasses, in: C. Massobrio, J. Du, M. Bernasconi, P.S. Salmon (Eds.), (Eds.), Molecular Dynamics Simulations of Disordered Materials: From Network Glasses to Phase-Change Memory Alloys, Springer International Publishing, Cham, 2015, pp. 157–180, https://doi.org/10.1007/978-3-319-15675-0_7.

[48] L. Huang, J. Kieffer, Challenges in modeling mixed ionic-covalent glass formers, in: C. Massobrio, J. Du, M. Bernasconi, P.S. Salmon (Eds.), (Eds.), Molecular Dynamics Simulations of Disordered Materials, Springer International Publishing, Cham, 2015, pp. 87–112, https://doi.org/10.1007/978-3-319-15675-0_4.

[49] C. Hermansen, J.C. Mauro, Y. Yue, A model for phosphate glass topology considering the modifying ion sub-network, J. Chem. Phys. 140 (2014), 154501, https://doi.org/10.1063/1.4870764.

[50] A.R. Potter, C.J. Wilkinson, S.H. Kim, J.C. Mauro, Effect of water on topological constraints in silica glass, Scr. Mater. 160 (2019) 48–52, https://doi.org/10.1016/j.scriptamat.2018.09.041.

[51] C.J. Wilkinson, Q. Zheng, L. Huang, J.C. Mauro, Topological constraint model for the elasticity of glass-forming systems, J. Non-Cryst. Solids 2 (2019), 100019, https://doi.org/10.1016/j.nocx.2019.100019.

[52] C. Hermansen, X. Guo, R.E. Youngman, J.C. Mauro, M.M. Smedskjaer, Y. Yue, Structure-topology-property correlations of sodium phosphosilicate glasses, J. Chem. Phys. 143 (2015), 064510, https://doi.org/10.1063/1.4928330.

[53] M.M. Smedskjaer, J.C. Mauro, R.E. Youngman, C.L. Hogue, M. Potuzak, Y. Yue, Topological principles of borosilicate glass chemistry, J. Phys. Chem. B. 115 (2011) 12930–12946, https://doi.org/10.1021/jp208796b.

[54] P. Boolchand, M. Bauchy, M. Micoulaut, C. Yildirim, Topological phases of chalcogenide glasses encoded in the melt dynamics, Physica Status Solidi (b) 255 (2018), 1800027, https://doi.org/10.1002/pssb.201800027.
[55] R. Chbeir, M. Bauchy, M. Micoulaut, P. Boolchand, Evidence for a correlation of melt fragility index with topological phases of multicomponent glasses, Front. Mater. 6 (2019), https://doi.org/10.3389/fmats.2019.00173.
[56] C. Mohanty, A. Mandal, V.K. Gogi, P. Chen, D. Novita, R. Chbeir, M. Bauchy, M. Micoulaut, P. Boolchand, Linking melt dynamics with topological phases and molecular structure of sodium phosphate glasses from calorimetry, Raman scattering, and infrared reflectance, Front. Mater. 6 (2019), https://doi.org/10.3389/fmats.2019.00069.